Mechanical switch for state transfer in dual-cavity optomechanical systems

Satya Sainadh U and Andal Narayanan*
Raman Research Institute, Bangalore, India
(Received 16 July 2013; published 3 September 2013)

Dual-cavity optoelectromechanical systems (OEMS) are those where two electromagnetic cavities are connected by a common mechanical spring. These systems have been shown to facilitate high-fidelity quantum-state transfer from one cavity to another. In this paper, we explicitly calculate the effect on the fidelity of state transfer when an additional spring is attached to only one of the cavities. Our quantitative estimates of loss of fidelity highlight the sensitivity of a dual-cavity OEMS when it couples to additional mechanical modes. We show that this sensitivity can be used to design an effective mechanical switch for inhibition or high-fidelity transmission of quantum states between the cavities.

DOI: 10.1103/PhysRevA.88.033802 PACS number(s): 42.50.Wk, 07.10.Cm

I. INTRODUCTION

A cornerstone optomechanical device is an optical cavity attached with a mechanical spring to one of its cavity surfaces. The dynamical back action resulting from the coupling of the cavity mode with the mechanical mode gives rise to a steady state, wherein the resonance frequency of the cavity and the spring constant of the spring are altered [1]. Rapid progress in this field was made after the experimental demonstration of cooling of the mechanical resonator to its quantum-mechanical ground state [2]. The question of the utility of such a device to store and transfer quantum states is an active area of experimental and theoretical investigation due to the ability of optoelectromechanical systems (OEMS) to interface between different information processing modules. Indeed, hybrid optoelectromechanical systems are fast becoming effective lossless interfacing devices.

A prototype optomechanical interface device was put forth by [3–6], which was subsequently experimentally realized [7]. The effectiveness of this interface device as a high-fidelity quantum-state-transfer device [5] is due to the existence of a dark state in the system Hamiltonian. This state does not include the mechanical mode, thus minimizing loss during state transfer. The dark state in such optomechanical systems is quite analogous to the dark state present in atomic systems, which exhibit the electromagnetically induced transparency (EIT) effect. Consequently, an optomechanically induced transparency (OMIT) effect was predicted [8] and observed [9] in these systems. The search for quantum optics effects in these systems has given rise to theoretical predictions of a wide variety of phenomena, including slowing down a probe light [10] and the electromagnetically induced absorption (EIA) [11] effect.

In this paper, we focus on the consequences of coupling an additional mechanical mode (spring 2) to one of the cavities of a dual-cavity OEMS architecture (Fig. 1). Such an analysis becomes highly relevant when compact optomechanical sensors like a silicon microdisk are being engineered [12] to interrogate another mechanical motion, like the motion of a cantilever in an atomic force microscope. The mechanical motion of the cantilever couples to the optical modes of the microdisk, which can then be read out. However, the microdisk itself supports mechanical modes of its own, whose frequencies can match that of the cantilever under study. In such systems, it is very pertinent to know how the microdisk's mechanical modes couple through its optical modes to the mechanical motion of the cantilever. This situation maps to the architecture of a single optical cavity coupled to two springs, which is a subset of our dual-spring–dual-cavity architecture (Fig. 1).

We show in this paper that even one additional mechanical mode coupled to one of the cavities in a dual-cavity OEMS can reduce the fidelity of state transfer below 0.5. This feature allows the use of the additional mechanical mode as a switch, which either enables or inhibits high-fidelity state transfer between cavities.

II. MODEL HAMILTONIAN

The dual-cavity–dual-spring system shown in Fig. 1 is described by the Hamiltonian ($\hbar = 1$)

$$\hat{H} = \sum_{i=1}^{2}[w_m \hat{a}_i^\dagger \hat{a}_i - \Delta_i \hat{d}_i^\dagger \hat{d}_i + G_i(\hat{a}_1^\dagger \hat{d}_i + \hat{a}_1 \hat{d}_i^\dagger)] + G_3(\hat{a}_2^\dagger \hat{d}_1 + \hat{a}_2 \hat{d}_1^\dagger). \quad (1)$$

The cavities represented by the annihilation operators $\hat{d}_i$ can both be optical cavities or, as is assumed in [13], one optical cavity and one microwave cavity. The optomechanical coupling of both the cavities with the springs $\hat{a}_i$ is provided by strong drive fields. w_m is the mechanical oscillation frequency of the springs, which is taken to be the same for both springs. The drive fields are red tuned with $\Delta_i = -w_m$. The coupling constants are denoted by $G_i = c_i g_i$, where c_i's are proportional to the amplitude of the drive fields and g_i's denote the single-photon coupling strength. g_i's are usually small, which results in the absence of quadratic cavity annihilation operator terms in the cavity coupling. Thus, the coupling of the cavity modes with the mechanical modes is linear [14,15] in the Hamiltonian. This Hamiltonian is written in a frame displaced by the strength $|c_i|^2$ of the drive fields and in the interaction picture. The internal losses of the cavities are denoted by κ_i and that of the springs by γ_i. We take the good cavity limit with $G_i \gg \kappa_i$ and work in the resolved sideband regime with $\kappa_i \ll w_m$.

*andal@rri.res.in

FIG. 1. (Color online) Schematic of the dual-spring–dual-cavity optomechanical system. The first cavity is attached to two springs.

In [13], the question of state transfer from cavity I to II was addressed when both the cavities were coupled to a single spring. However, in realistic systems, there might be additional mechanical modes to which the cavity modes couple asymmetrically. In this paper, we address this question by considering explicit coupling of the first cavity to another spring (denoted by 2 in Fig. 1). To simplify the calculation, we have made spring 2 identical to spring 1.

III. DYNAMICAL EVOLUTION

For explicitly studying the dynamical evolution of both cavity modes, we consider the hybrid scheme of [13], wherein the couplings G_i are turned on simultaneously. In the hybrid scheme, there is equal participation of dark and bright modes during state transfer. In our architecture, due to the additional coupling, no dark state for the system Hamiltonian exists. In our calculations, we consider $G_1 = G_2 = G$ with $G_3 = pG$, where p is a tunable parameter.

The absence of dark modes in the system's eigenstates results in the mixing of cavity modes and mechanical modes during dynamical evolution of the system. Thus the states of the cavity modes cannot be swapped with each other due to the contribution from mechanical modes. To explicitly see this, we evolve the cavity modes and mechanical modes using Heisenberg equations of motion in the absence of cavity dissipation κ_i and mechanical dissipation γ_i. These are given by

$$e^{iw_m t}\hat{d}_2(t) = \hat{d}_2(0)\left(\frac{\nu_-\cos\left(\frac{h_+t}{4}\right)+\nu_+\cos\left(\frac{h_-t}{4}\right)}{2}\right)+\hat{a}_2(0)\frac{4ipG}{\sqrt{4+p^4}}\left(\frac{\sin\left(\frac{h_-t}{4}\right)}{h_-}-\frac{\sin\left(\frac{h_+t}{4}\right)}{h_+}\right)+\hat{d}_1(0)\left(\frac{\cos\left(\frac{h_+t}{4}\right)-\cos\left(\frac{h_-t}{4}\right)}{\sqrt{4+p^4}}\right)$$
$$-\hat{a}_1(0)(2iG)\left[\left(\nu_-+\frac{2}{\sqrt{4+p^4}}\right)\frac{\sin\left(\frac{h_+t}{4}\right)}{h_+}+\left(\nu_+-\frac{2}{\sqrt{4+p^4}}\right)\frac{\sin\left(\frac{h_-t}{4}\right)}{h_-}\right], \tag{2a}$$

$$e^{iw_m t}\hat{d}_1(t) = \hat{d}_1(0)\left(\frac{\nu_-\cos\left(\frac{h_-t}{4}\right)+\nu_+\cos\left(\frac{h_+t}{4}\right)}{2}\right)+\hat{a}_1(0)\frac{i}{4G\sqrt{4+p^4}}\left[h_-\sin\left(\frac{h_-t}{4}\right)-h_+\sin\left(\frac{h_+t}{4}\right)\right]$$
$$+\hat{d}_2(0)\left(\frac{\cos\left(\frac{h_+t}{4}\right)-\cos\left(\frac{h_-t}{4}\right)}{\sqrt{4+p^4}}\right)-\hat{a}_2(0)(2iGp)\left(\nu_-\frac{\sin\left(\frac{h_-t}{4}\right)}{h_-}+\nu_+\frac{\sin\left(\frac{h_+t}{4}\right)}{h_+}\right), \tag{2b}$$

where $\nu_\pm = 1 \pm \frac{p^2}{\sqrt{4+p^4}}$, $h_\pm = \sqrt{8G^2(2+p^2\pm\sqrt{4+p^4})}$.

We see from Eq. (2a) that at all times, there is a nonvanishing contribution of $\hat{a}_i$ to the state of the second cavity $\hat{d}_2$. To address the question of state transfer we choose an optimum time given by $t_0 = 4\pi/h_+$. For values of $p \gg 1$, we have $\hat{d}_2(t_0) \approx \hat{d}_2(0)$ and $\hat{d}_1(t_0) \approx \hat{d}_1(0)$. So it is clear that when the additional mechanical mode is strongly coupled to one of the cavity modes, the state transfer gets totally inhibited. More importantly, we also see that the cavities retain the initial state in which they were prepared. For small values of p and for the particular case of $p = 0$, at appropriate time t_0, we find $\hat{d}_1(t_0) = -\hat{d}_2(0)$ and $\hat{d}_2(t_0) = -\hat{d}_1(0)$ (neglecting phase factors), thus recovering the results of the hybrid scheme.

We exploit this sensitivity of fidelity to additional mechanical modes in a dual-cavity OEMS to outline a design for a mechanically mediated switch. This switch will facilitate high-fidelity state transfer or totally inhibit it. For practical implementation of this effect, we need an additional spring 2, whose spring constant can be varied externally. This can be done, for example, through application of an external voltage. Initially, spring 2 is kept floppy so that no effective optomechanical coupling is established. Thus state transfer between cavities proceed with high fidelity through spring 1. Then by application of an external voltage the spring acquires a voltage-dependent stiffness which establishes effective optomechanical coupling. This, as we rigorously show below, reduces the fidelity of state transfer. We understand that electrostatic spring-softening and -stiffening structures are already available in the field of micro-electro-mechanical systems (MEMS) [16], thus making practical implementation of this idea feasible.

Alternately, the coupling of spring 2 to cavity I can also be modified through its single-photon optomechanical coupling parameter g_0, where $g_0 = x_{\mathrm{ZPF}}\frac{\partial\omega_{\mathrm{cavity}}}{\partial x}$, with $x_{\mathrm{ZPF}} = \sqrt{\frac{\hbar}{2m\omega_m}}$. As is shown in [17], it is possible to tune g_0 of a cavity-spring system through two orders of magnitude. So if we use this architecture to fabricate our dual-cavity–dual-spring system, then we can achieve a large tuning range for p.

In the following section, we show detailed calculations of fidelity for intracavity state transfer for input Gaussian states in cavity I in our dual-spring–dual-cavity architecture (Fig. 1).

IV. FIDELITY CALCULATION FOR INPUT GAUSSIAN STATES

In this section, we give the details of our calculations and present the results for transfer fidelity for input Gaussian states. The input states are represented using Wigner functions, and their dynamical evolution is calculated using the Lindblad

model for dissipation. The cavity and spring systems are assumed to be in a bath at temperature T. The bath modes couple to the system modes, giving rise to the density matrix $\hat{R}$, which evolves according to the equation $\dot{\hat{R}} = -i[\hat{H},\hat{R}]$. The reduced density matrix $\hat{\rho}$, corresponding to the resonator and cavity modes, is obtained upon tracing out the bath degrees of freedom. $\hat{\rho}$ is expressed using the quadrature modes of cavity (c) and resonator (m) as $\hat{\boldsymbol{X}}^T \equiv (\hat{x}_{c_k},\hat{p}_{c_k},\ldots,\hat{x}_{m_k},\hat{p}_{m_k})$, with $\hat{x}_{c_k} = \frac{\hat{d}_k+\hat{d}_k^\dagger}{2}$, $\hat{x}_{m_k} = \frac{\hat{a}_k+\hat{a}_k^\dagger}{2}$ and $\hat{p}_{c_k} = -i\frac{\hat{d}_k-\hat{d}_k^\dagger}{2}$, $\hat{p}_{m_k} = -i\frac{\hat{a}_k+\hat{a}_k^\dagger}{2}$, where k can be 1/I or 2/II. The effective master equation for the reduced density matrix corresponding to the bilinear Hamiltonian form is given by

$$\dot{\hat{\rho}} = -i[\hat{\boldsymbol{X}}^T \boldsymbol{H} \hat{\boldsymbol{X}},\hat{\rho}] + \sum_j \left[\frac{\Gamma_{j_+}}{2}\mathcal{D}\big(\hat{\boldsymbol{L}}_j^T\hat{\boldsymbol{X}}\big) + \frac{\Gamma_{j_-}}{2}\mathcal{D}\big(\hat{\boldsymbol{L}}_j^T\hat{\boldsymbol{X}}\big)^\dagger\right]\hat{\rho}. \tag{3}$$

$\mathcal{D}(\hat{O})\hat{\rho} \equiv 2\hat{O}\hat{\rho}\hat{O}^\dagger - \hat{O}^\dagger\hat{O}\hat{\rho} - \hat{\rho}\hat{O}^\dagger\hat{O}$ is the Lindblad superoperator. $\hat{\boldsymbol{L}}_j^T\hat{\boldsymbol{X}}$ corresponds to the mode annihilation operators of both the cavities and the springs. $\Gamma_{j_\mp}$ denotes the rate of loss or amplification of energy from the bath into the system's jth mode, where j can be $c_{\mathrm{I/II}}(m_{1/2})$, corresponding to the first or second cavity (mechanical resonator). We consider the symmetric-cavity case of $\kappa_1 = \kappa_2 = \kappa$. We also consider similar decay parameters for both the springs with $\gamma_1 = \gamma_2 = \gamma$. For simplicity, we consider the average number of thermal quanta exchanged by both the cavities with the bath to be the same. The same holds true even for the springs, i.e., $N_{c_\mathrm{I}} = N_{c_\mathrm{II}} = N_c$ and $N_{m_1} = N_{m_2} = N_m$. With these parameters, we have $\Gamma_{c_k-} = N_c\kappa$, $\Gamma_{m_k-} = N_m\gamma$, $\Gamma_{c_k+} = (N_c+1)\kappa$, and $\Gamma_{m_k+} = (N_m+1)\gamma$.

We express the initial single-mode Gaussian state in cavity I as a Wigner function $W_i(\boldsymbol{X})$. The Wigner function is characterized by the first moment of the mode quadratures $\overline{\boldsymbol{X}}_i$ and their covariance matrix $\boldsymbol{\sigma}_i$. From Eq. (3), one can evolve $\overline{\boldsymbol{X}}$ and $\boldsymbol{\sigma}$ as

$$\frac{d\overline{\boldsymbol{X}}}{dt} = \mathcal{Q}\overline{\boldsymbol{X}}, \quad \frac{d\boldsymbol{\sigma}}{dt} = \mathcal{Q}\boldsymbol{\sigma} + \boldsymbol{\sigma}\mathcal{Q}^T + \mathcal{N}. \tag{4}$$

The matrices $\mathcal{Q}$ and $\mathcal{N}$ are given by

$$\mathcal{Q} = \begin{pmatrix} -\kappa/2 & 0 & 0 & 0 & 0 & G & 0 & pG \\ 0 & -\kappa/2 & 0 & 0 & -G & 0 & -pG & 0 \\ 0 & 0 & -\kappa/2 & 0 & 0 & G & 0 & 0 \\ 0 & 0 & 0 & -\kappa/2 & -G & 0 & 0 & 0 \\ 0 & G & 0 & G & -\gamma/2 & 0 & 0 & 0 \\ -G & 0 & -G & 0 & 0 & -\gamma/2 & 0 & 0 \\ 0 & pG & 0 & 0 & 0 & 0 & -\gamma/2 & 0 \\ -pG & 0 & 0 & 0 & 0 & 0 & 0 & -\gamma/2 \end{pmatrix}, \quad \mathcal{N} = \frac{1}{4}\mathrm{Diag}\{\overline{\boldsymbol{\kappa}},\overline{\boldsymbol{\kappa}},\overline{\boldsymbol{\kappa}},\overline{\boldsymbol{\kappa}},\overline{\boldsymbol{\gamma}},\overline{\boldsymbol{\gamma}},\overline{\boldsymbol{\gamma}},\overline{\boldsymbol{\gamma}}\}, \tag{5}$$

which is a diagonal matrix, with $\overline{\boldsymbol{\kappa}} = \kappa(2N_c+1)$ and $\overline{\boldsymbol{\gamma}} = \gamma(2N_m+1)$. The matrix $\mathcal{Q}$ is responsible for the evolution of the system under the Hamiltonian including the intrinsic damping terms, while the matrix $\mathcal{N}$ consists solely of the bath parameters that determine the effect of the bath on the system. Evolving the initial state $W_i(\boldsymbol{X})$, using Eqs. (3)–(5), we arrive at the final state $W_f(\boldsymbol{X})$ at time t_0 in cavity II. The fidelity between these initial (i) and final (f) single-mode Gaussian states is given by

$$F = \frac{1}{1+\overline{n}_h}\exp\left(-\frac{\lambda^2}{1+\overline{n}_h}\right), \tag{6a}$$

$$\overline{n}_h = 2\sqrt{\mathrm{Det}[\boldsymbol{\sigma_i}+\boldsymbol{\sigma_f}]} - 1, \tag{6b}$$

$$\lambda^2 = (\overline{\boldsymbol{X}}_{\boldsymbol{i}} - \overline{\boldsymbol{X}}_{\boldsymbol{f}})\cdot\frac{\sqrt{\mathrm{Det}[\boldsymbol{\sigma_i}+\boldsymbol{\sigma_f}]}}{\boldsymbol{\sigma_i}+\boldsymbol{\sigma_f}}\cdot(\overline{\boldsymbol{X}}_{\boldsymbol{i}} - \overline{\boldsymbol{X}}_{\boldsymbol{f}}). \tag{6c}$$

For simplicity, we consider the initial state to be a squeezed state given by

$$|\alpha,r\rangle = \hat{D}(\alpha)\hat{S}(r)|0\rangle, \tag{7}$$

with

$$\hat{S}(r) = \exp\left(\frac{r}{2}\hat{d}_1^2 - \frac{r}{2}\hat{d}_1^{\dagger 2}\right), \tag{8}$$

where r is real and

$$\hat{D}(\alpha) = \exp(\alpha\hat{d}_1^\dagger - \alpha^*\hat{d}_1), \tag{9}$$

with $\alpha = |\alpha|e^{i\phi}$. Therefore the covariance matrix and first moment of the quadratures are given by

$$\overline{\boldsymbol{X}}_{\boldsymbol{i}} = \begin{pmatrix} |\alpha|\cos\phi \\ |\alpha|\sin\phi \end{pmatrix}, \qquad \boldsymbol{\sigma_i} = \frac{1}{4}\begin{pmatrix} e^{-2r} & 0 \\ 0 & e^{2r} \end{pmatrix}. \tag{10}$$

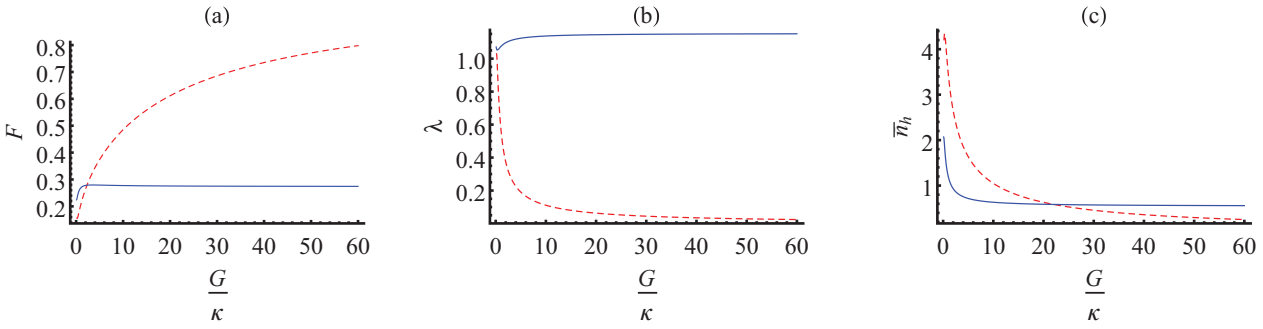

FIG. 2. (Color online) (a) Fidelity F, (b) amplitude decay λ, and (c) heat exchange with the bath $\overline{n}_h$ as a function of coupling strength $\frac{G}{\kappa}$. These graphs are drawn for an initial squeezed state with squeezing parameter $r = 1$, with $|\alpha| = 1$, $\phi = \frac{\pi}{4}$, and with $p = 5$ (thick blue solid line). In all three graphs a comparison plot is drawn for $p = 0$ (red dashed line), which is the case where the extra spring 2 is absent. The graphs are plotted for experimentally realizable parameters, which are $\gamma = \frac{1}{50}\kappa = 2\pi \times 1$ kHz and $\omega_m = 2\pi \times 10$ MHz with the symmetric cavity condition, i.e., $N_{\rm I} = N_{\rm II} = N_c$, calculating for $\omega_{\rm cavity} = 2\pi \times 10$ GHz at $T_{\rm bath} = 1.5$ K.

Based on the mathematical formulation outlined above, we calculate the first moment and covariance matrix for the output state. These work out to be

$$\overline{\boldsymbol{X}}_f = \underbrace{e^{-\frac{\kappa+\gamma}{4}t_0}\left(\frac{1+A_-}{\sqrt{4+p^4}}\right)}_{C_1}\overline{\boldsymbol{X}}_i, \tag{11}$$

$$\boldsymbol{\sigma}_f = \underbrace{\left(e^{-\frac{\kappa+\gamma}{2}t_0}\left\{\frac{1}{16}[\nu_- - \nu_+ A_-(t_0)]^2 + \frac{2G^2}{h_-^2}\left(\nu_+ - \frac{2}{\sqrt{4+p^4}}\right)\sin^2\left(\frac{h_- t_0}{4}\right)\right\} + \overline{\boldsymbol{\kappa}}\,(\nu_+\mathcal{I}_{2_-} + \nu_-\mathcal{I}_{2_+}) + \frac{2\overline{\boldsymbol{\gamma}}}{(h_+h_-)^2}\left[\beta(\nu_-\mathcal{I}_{1_+} + \nu_+\mathcal{I}_{1_-}) + \frac{2G^2(\kappa-\gamma)^2}{\sqrt{4+p^4}}(\mathcal{I}_{1_-} - \mathcal{I}_{1_+})\right]\right)}_{C_2}\boldsymbol{I} + \underbrace{e^{-\frac{\kappa+\gamma}{2}t_0}\left(\frac{1+A_-}{\sqrt{4+p^4}}\right)^2}_{C_3}\boldsymbol{\sigma_i}, \tag{12}$$

with the expressions $\beta = G^2[16G^2p^2 - (\kappa-\gamma)^2]$, $A_\pm(t) = \cos(\frac{h_\pm t}{4}) - \frac{\kappa-\gamma}{h_\pm}\sin(\frac{h_\pm t}{4})$ and the integrals $\mathcal{I}_{1_\pm} = \int_0^{t_0} e^{-\frac{\kappa+\gamma}{2}t}\sin^2(\frac{h_\pm t}{4})dt$, $\mathcal{I}_{2_\pm} = \int_0^{t_0} e^{-\frac{\kappa+\gamma}{2}t}A_\pm^2 dt$. Identifying the coefficients of $\overline{\boldsymbol{X}}_i$, the identity matrix $\boldsymbol{I}$, and $\boldsymbol{\sigma_i}$ as C_1,C_2, and C_3 respectively, we have

$$\overline{n}_h = \frac{1}{2}\sqrt{(1+C_3)^2 + 16C_2^2 + 8C_2(1+C_3)\cosh(2r)} - 1 \tag{13}$$

$$\lambda^2 = \frac{2(1-C_1)^2|\alpha|^2}{\overline{n}_h + 1}\left[C_2 + \frac{(1+C_3)}{4}(e^{2r}\cos^2\phi + e^{-2r}\sin^2\phi)\right]. \tag{14}$$

We see from the graph for fidelity [Fig. 2(a)] that, with the additional spring, the fidelity falls to values below 0.3 for strong couplings over a wide range. The loss of fidelity is mainly due to the decay of amplitude, denoted by the parameter λ [Fig. 2(b)], rather than from heat exchange with the bath, denoted by $\overline{n}_h$ [Fig. 2(c)].

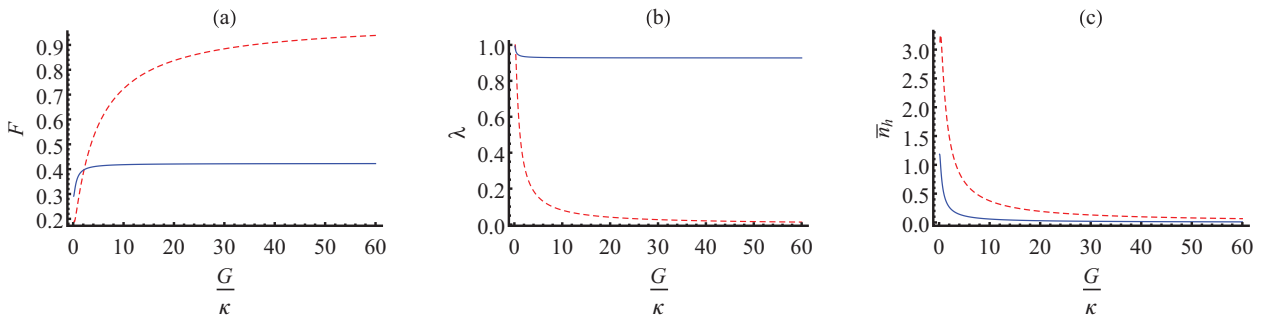

FIG. 3. (Color online) (a) Fidelity F, (b) λ, and (c) $\overline{n}_h$ as a function of coupling strength $\frac{G}{\kappa}$ for a coherent state with $r = 0$, $\alpha = 1$ and for $p = 5$ (thick blue solid line). Shown also in each graph is a plot for $p = 0$ (red dashed line), which signifies the absence of the extra spring. The graphs are plotted for experimentally realizable parameters, where $\gamma = \frac{1}{50}\kappa = 2\pi \times 1$ kHz and $\omega_m = 2\pi \times 10$ MHz with the symmetric cavity condition, i.e., $N_{\rm I} = N_{\rm II} = N_c$, calculating for $\omega_{\rm cavity} = 2\pi \times 10$ GHz at $T_{\rm bath} = 1.5$ K.

Figures 3(a)–3(c) show fidelity, amplitude decay, and heat exchange as a function of $\frac{G}{\kappa}$ for state transfer from cavity I to cavity II for an input coherent state with $|\alpha| = 1$ for $p = 5$. Comparing with the corresponding graphs in Fig. 2, we see that, qualitatively, the coherent state exhibits similar features to the squeezed state. Our calculations show that, for higher values of p, the fidelity for coherent states reaches a limiting value of $(\frac{1}{e})^{|\alpha|^2}$ and is insensitive to the decay parameters of the cavity and spring. In addition, for input coherent states, at very low bath temperatures around 0 K, the heating parameter $\overline{n}_h \rightarrow 0$, but the amplitude decay λ is $\approx$0.9. These features enable the action of the mechanical spring as a switch to function with cavities of varying finesse and also at very low ambient temperatures [18].

V. CONCLUSIONS

Dual-cavity OEMS are fast becoming model systems for high-fidelity quantum-state transfer. In this paper, we analyze and answer the very pertinent question of the fidelity of state transfer when one of the cavities of this model system is coupled to an extra mechanical mode. We show that the fidelity drops to a value below 0.5 for a wide range of values of coupling strength and decay parameters. This highlights the need to isolate all spurious mechanical couplings in the design of interface optomechanical architectures. Based on our calculations, we propose a mechanical switch which will either enable or inhibit high-fidelity state transfer. We envisage that the switch can be made out of state-of-the-art MEMS actuators working on the electrostatic spring-softening mechanism.

[1] T. Kippenberg and K. Vahala, Science **321**, 1172 (2008).

[2] A. D. OConnell, M. Hofheinz, M. Ansmann, R. C. Bialczak, M. Lenander, E. Lucero, M. Neeley, D. Sank, H. Wang, M. Weides *et al.*, Nature (London) **464**, 697 (2010).

[3] L. Tian and H. Wang, Phys. Rev. A **82**, 053806 (2010).

[4] C. A. Regal and K. W. Lehnert, J. Phys.: Conf. Ser. **264**, 012025 (2011).

[5] V. Fiore, Y. Yang, M. C. Kuzyk, R. Barbour, L. Tian, and H. Wang, Phys. Rev. Lett. **107**, 133601 (2011).

[6] Y.-D. Wang and A. A. Clerk, Phys. Rev. Lett. **108**, 153603 (2012).

[7] J. Chan, T. M. Alegre, A. H. Safavi-Naeini, J. T. Hill, A. Krause, S. Gröblacher, M. Aspelmeyer, and O. Painter, Nature (London) **478**, 89 (2011).

[8] G. S. Agarwal and S. Huang, Phys. Rev. A **81**, 041803 (2010).

[9] S. Weis, R. Rivière, S. Deléglise, E. Gavartin, O. Arcizet, A. Schliesser, and T. J. Kippenberg, Science **330**, 1520 (2010).

[10] D. Tarhan, S. Huang, and Ö. E. Müstecaplıoğlu, Phys. Rev. A **87**, 013824 (2013).

[11] K. Qu and G. S. Agarwal, Phys. Rev. A **87**, 031802 (2013).

[12] Y. Liu, H. Miao, V. Aksyuk, and K. Srinivasan, Opt. Express **20**, 18268 (2012).

[13] Y.-D. Wang and A. A. Clerk, New J. Phys. **14**, 105010 (2012).

[14] I. Wilson-Rae, N. Nooshi, W. Zwerger, and T. J. Kippenberg, Phys. Rev. Lett. **99**, 093901 (2007).

[15] F. Marquardt, J. P. Chen, A. A. Clerk, and S. M. Girvin, Phys. Rev. Lett. **99**, 093902 (2007).

[16] Y. Zhao, F. E. H. Tay, G. Zhou, and F. Siong Chau, Optik (Munich, Ger.) **117**, 367 (2006).

[17] H. Miao, K. Srinivasan, and V. Aksyuk, New J. Phys. **14**, 075015 (2012).

[18] T. P. Purdy, D. W. C. Brooks, T. Botter, N. Brahms, Z.-Y. Ma, and D. M. Stamper-Kurn, Phys. Rev. Lett. **105**, 133602 (2010).